CHEMPHYSCHEM

DOI: 10.1002/cphc.200800851

Spectroscopy and Defect Identification for Fluorinated Carbon Nanotubes

Carla Bittencourt,*[a] Gregory Van Lier,[b] Xiaoxing Ke,[c] Irene Suarez-Martinez,[d] Alexandre Felten,[e] Jacques Ghijsen,[e] Gustaaf Van Tendeloo,[c] and Christopher P. Ewels[d]

Multi-wall carbon nanotubes (MWCNTs) were exposed to a CF_4 radio-frequency (rf) plasma. High-resolution photoelectron spectroscopy shows that the treatment effectively grafts fluorine atoms onto the MWCNTs, altering the valence electronic states. Fluorine surface concentration can be tuned by varying the exposure time. Evaporation of gold onto MWCNTs is used to mark active site formation. High-resolution transmission electron microscopy coupled with density functional theory (DFT) modelling is used to characterise the surface defects formed, indicating that the plasma treatment does not etch the tube surface. We suggest that this combination of theory and microscopy of thermally evaporated gold atoms onto the CNT surface may be a powerful approach to characterise both surface defect density as well as defect type.

1. Introduction

Fluorination is a promising method for expanding the use of carbon nanotubes (CNTs) to several areas where the tailoring of properties such as wettability, adhesion, chemical stability, permeation, electrical conductivity, and biocompatibility are important.[1] Due to fluorine's high electronegativity, fluorination drastically modifies the nanotube surface chemistry, changing the electronic properties depending on the degree of fluorination and the specific addition pattern of the fluorine atoms on the nanotube surface. In fluorinated graphite, the electrical conduction can be enhanced by promoting ionic bonding between fluorine and carbon atoms that increases the number of hole carriers, whereas covalent bonding produces a decrease in the overall carrier concentration.[2] In CNTs, different fluorine addition patterns occur for gas phase fluorination depending on the functionalization temperature: below 200 °C the pattern approaches C_4F, increasing to a maximal C_2F surface coverage between around 250 °C and 300 °C, and with temperatures above ~300 °C destruction of the nanotube lattice where coverage can approach CF.[3,4] The electrical conductivity of CNTs was reported to decrease after gas-phase fluorine functionalization; while pristine CNTs were good conductors, tubes fluorinated at temperatures of 250 °C and above were insulators.[5–7] By using density functional calculations, Ewels et al.[8] showed that this transition temperature arises from the surface migration barrier for fluorine atoms on tube surfaces, to pass through next-neighbour sites which blocks dense packing and fluorine banding at low temperatures. This was associated to the transition from "semi-ionic" low-coverage to covalent high-coverage fluorination.[8,9] Surface fluorine atoms were found to migrate rapidly at low temperatures before pairing up at third-neighbour spacing. We note that the term "semi-ionic" sometimes applied to this phase is somewhat misleading, because although the C–F bonds are dilated, they remain covalent in this arrangement.[8] For this reason, rather than using the terms "semi-ionic" and covalent for these different bonding arrangements, we prefer low- and high-density packing respectively. Fluorine coverage at the third neighbour is limited to a maximum F/C surface ratio of 0.25. As the temperature reaches ~200–250 °C, fluorine can overcome the activation barrier associated with adopting the energetically less favourable second-neighbour configuration, enabling a phase with close packing at the first neighbour, until finally arriving to a F/C ratio of 0.5 under further fluorine addition.[8]

Fluorination in fluorine gas generally results in a high reaction ratio and a deep penetration into carbon-related materials which prevents a good control of sidewall fluorination.[10] In this context, plasma fluorination has the potential to limit the fluorination area to the external surface of the nanotubes if performed at room temperature; in addition it requires a reaction time orders of magnitude shorter than other fluorination methods.[11,12] Earlier, we showed that CF_4 rf plasma treatment performed at low applied power grafts fluorine atoms at the CNT surface without inducing significant etching, nevertheless

[a] Dr. C. Bittencourt
University of Mons-Hainaut
Parc Initialis, Av. Nicolas Copernic 1, Mons 7000 (Belgium)
Fax: (+32) 65373841
E-mail: carla.bittencourt@umh.ac.be

[b] Dr. G. Van Lier
Research Group of General Chemistry (ALGC)
Free University of Brussels - Vrije Universiteit Brussel (VUB)
Pleinlaan 2, B-1050, Brussels (Belgium)

[c] X. Ke, Prof. G. Van Tendeloo
University of Antwerp, EMAT
Groenenborgerlaan 171, B2020 Antwerpen (Belgium)

[d] Dr. I. Suarez-Martinez, Dr. C. P. Ewels
IMN, CNRS UMR6502
Université de Nantes
BP 32229, 44322 Nantes (France)

[e] Dr. A. Felten, Dr. J. Ghijsen
University of Namur, LISE
61 rue de Bruxelles, Namur 5000, Namur (Belgium)

the number of active sites for metal nucleation at the CNT surface increased.[13] It remains unclear exactly which surface defect species are produced in such potentially aggressive surface treatments and whether they are associated with etching of surface carbon atoms. It is one of our aims to clarify this question.

Herein, CF_4 plasma functionalization of multiwall carbon nanotubes are investigated by combining high-resolution X-ray photoelectron spectroscopy with high-resolution electron microscopy and density functional calculations. In the plasma the non-reactive CF_4 gas is converted into highly reactive fluorine species that are accelerated by the electric field and interact with the CNTs. The evolution of the F/C ratio for increasing functionalization time and the nature of the C–F bonds is studied by high-resolution synchrotron based X-ray photoelectron spectroscopy (XPS) and the integrity of the surface is evaluated by high-resolution electron microscopy. Defect labelling is attempted by evaporating gold atoms onto the CNT surface and quantified by high-resolution transmission electron microscopy (HRTEM).[14] The dispersion of metal clusters that weakly interact with the CNT surface (such as gold) can be used to monitor the presence of active sites such as morphological and/or chemical defects as well as their distribution.[14] On the graphitic surface, transition-metal atoms are mobile and form clusters as the cohesive energy of these metals is much larger than the adsorption enthalpy—nucleation is characterized by diffusion-limited aggregation.[15] The nucleation centres were reported to be defects (chemical or structural) at the surface,[16] but it is not a priori obvious what such surface defect species will be. In order to understand the interaction between gold and different fluorinated defect species, we used density functional calculations to model a range of fluorinated surface defects on both pristine and etched graphene sheets, and examined their interaction with individual gold atoms.

Experimental Section

Samples were prepared using commercial MWCNT powder (average inner diameter: 5 nm, outer diameter: 15 nm, corresponding to 14 or 15 concentric layers and an average length of ca. 20 μm) synthesized via catalytic chemical vapour deposition (CCVD).[17] The functionalization was performed in a homemade chamber using inductive coupled plasma at the RF frequency of 13.56 MHz.[11] A controlled flow of CF_4 was introduced inside the chamber; the treatment was performed at gas pressure of 0.1 Torr, using 10 W.

Samples for XPS, ultraviolet photoelectron spectroscopy (UPS) and TEM were plasma-treated simultaneously: for the XPS and UPS analysis the MWCNT powder was supported on a copper conductive tape suitable for ultra-high vacuum. For TEM analysis the CNT powder was dispersed in ethanol and the solution was dropped onto a lace-like carbon film supported by a copper grid. The samples were treated on their support in order to avoid post-treatment contamination.

Gold was thermally evaporated from a gold wire. A quartz balance was used to calibrate the evaporation rate with an accuracy of 0.2 Å min^{-1}.

HRTEM was performed using a Philips CM30 microscope at 200 kV. The changes induced in the CNT electronic states due to the grafting of fluorine atoms by the rf plasma treatment were investigated by XPS. X-ray photoemission experiments were performed at UE56 beam line BESSY II (Berlin) using the Mustang end-station. The nominal resolution of the system (source plus analyzer) was 0.1 eV.[18] Photon energies were selected so that all spectra were recorded at similar kinetic energies corresponding to high surface sensitivity, namely 400 eV for recording C 1s, 800 eV for F 1s, and 110 eV for valence bands. The selected photon energy for valence band studies, together with a favourable cross-section ratio,[19] lead to a higher contribution of the fluorine states on the valence band spectra. The Au $4f_{7/2}$ peak at 84.0 eV binding energy, recorded on a reference sample, was used for calibration of the binding energy scale.

Density Functional calculations within the Local Density Approximation[20] are carried out on an 8×8 supercell of graphene, that is, a monolayer of 128 carbon atoms. Fully spin-polarized single k-point calculations were geometrically optimized from multiple possible starting structures. Hartwigsen–Goedecker–Hutter (HGH) relativistic pseudopotentials[21] were used for all atoms. Atom-centered Gaussian basis functions were used to construct the many-electron wave function with angular momenta up to $l=2$. Electronic level occupation was obtained using a Fermi occupation function with $kT=0.04$ eV. In the energy analysis that follows, absolute binding energies are defined as the difference in energy between the relaxed combined system, and that of the isolated perfect graphite sheet and a single isolated metal atom ($s=1$), unless stated otherwise.

2. Results

We first characterise the results of the fluorination treatment using photoelectron spectroscopy. Table 1 presents the parameters used for the plasma treatment and the resulting F/C ratio evaluated by XPS analysis. As mentioned before, the photon excitation energy was chosen to generate photoelectrons with kinetic energy of the order of 100 eV (high surface sensitivity). At this kinetic energy, the inelastic electron mean free path was reported to be ~5 Å.[22] Therefore, considering the distance between the CNT walls (~3.45 Å); only photoelectrons generated in the two outer walls will have enough

Table 1. Parameters used for the plasma treatment of MWCNTs, together with the F/C ratio evaluated by XPS and the actual surface coverage on the outer wall. Samples were treated using a RF-plasma at CF_4 gas pressure of 0.1 Torr and 10 W. The F/C ratio as determined by XPS includes contribution of photoelectrons belonging to the two outer walls, so the quoted fluorine/carbon ratio of the surface is twice the measured F/C ratio.

Sample	Treatment time [s]	F/C (XPS)	F/C ratio coverage of the outer wall
1	2	0.25	0.50
2	5	0.22	0.44
3	15	0.19	0.38
4	30	0.16	0.32
5	45	0.17	0.34
6	60	0.16	0.32
7	300	0.12	0.24

energy to travel through the sample, overcome the surface barrier and escape into the vacuum, thus contributing to the photoemission peak. Thus, the F/C ratio as determined by XPS includes contribution of photoelectrons belonging to the two outer walls, meaning that the actual fluorine/carbon ratio of the surface will be twice the measured F/C ratio.

The chemical modification induced by the plasma treatment at the CNT surface can easily be identified by analyzing core-level spectra. The C 1s region XPS spectra for pristine and functionalized CNTs are shown in Figure 1. The peak at 284.6 eV is

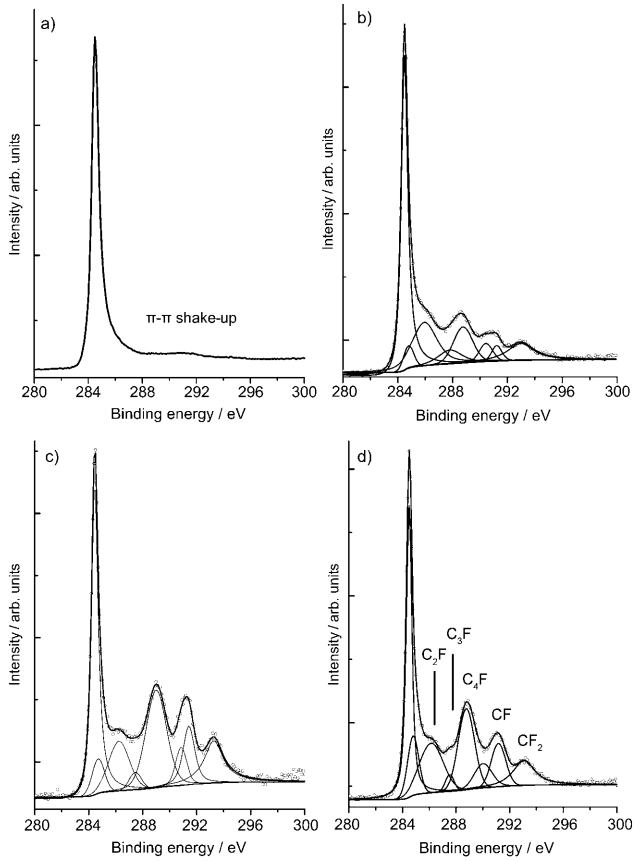

Figure 1. Carbon 1s XPS spectrum recorded using $h\nu = 400$ eV on a) pristine MWCNTs and on CF_4 plasma functionalized for b) 2 s, c) 60 s and d) 300 s. Spectra normalised to give the same primary peak height.

generated by photoelectrons emitted from the C 1s core level of carbon atoms whereas the low intensity and wide structure around 290 eV is due to the π–π shake-up process.[23] Chemical modification by the plasma treatment is revealed by the appearance of new structures contributing to the C 1s line shape at higher binding energies. These structures are generated by photoelectrons emitted from carbon atoms participating in C–F bonding (primary components) or from a carbon atom neighbour to a carbon atom bound to a fluorine (inductive components). Due to its high electronegativity, fluorine has a very strong effect on the electronic screening of the element to which it is bound. In addition, when a carbon atom not bound to fluorine is first neighbour of another carbon atom bound to one or several fluorine atoms, an inductive effect arises.[24] The main peak in the C 1s spectrum of the plasma functionalized samples is generated by photoelectrons emitted from the carbon atoms that do not interact directly with fluorine atoms. It can be decomposed into two components (Figure 1 b). The asymmetric component (1), which is common in metallic samples, is due to the interaction between the photohole created during the photoemission process and the conduction electrons. The second component (2) is an inductive component. The reported primary binding energy BE shifts in the C 1s level of CF_n groups ($n = 1$–3) correspond to the following ranges: 3–4.8, 6–7.5, 7.5–10 eV, according to the number of fluorine atoms bound to the carbon concerned, that is, one, two or three, respectively.[22] The importance of the inductive effect appears from the differences in binding energy observed for carbon atoms with different environments: for instance the C 1s BE of a carbon atom not directly bound to an fluorine atom, but a first neighbour of CF_n ($n = 1$–3) groups, is shifted of 0.6 ± 0.2 eV when the given carbon atom is bound to only one CF group, and of 1.4 ± 0.2 eV when its neighbours are either two CF groups or one CF_2 group. From these reported results we can suggest the following attribution for the peaks observed in Figure 1: C_2F at 286.4 eV, C_3F at 287.5 eV, C_4F at 288.8 eV, CF at 291.0 eV, and CF_2 at 293.0 eV.

From Table 1, we can see that a maximum F/C ratio of 0.25 (equivalent to C_2F surface coverage) is obtained after 2 s of functionalization; for increasing functionalization times, this ratio is reduced. Figure 1 shows that for increasing functionalization times, the relative intensity of the different components varies. This trend suggests that certain bond configurations are more stable and/or are less influenced by the interaction with the CF_4 plasma. We believe that the reduction in the F/C ratio for increasing functionalization time is mainly due to the chemical interaction between the CF_4 plasma and the less stable bond configuration—fluorine plasmas are characterized by high-rate chemical interaction.[25] As the ions in the plasma interacts with carbon atoms in the graphite layer of MWCNTs, fluorine atoms can either bond to carbon atoms or cut C–C bonds. The former forms C–F bonds while leaving graphite layers unchanged, while the latter can lead to vacancy formation and collapse of graphitic layers.

Figure 2 shows the F 1s core level spectrum recorded on the sample functionalized for 300 s. No major change was observed in the spectrum line from 2 s to 300 s of functionalization. At the onset of the treatment (2 s), the F 1s peak is symmetrical and centred at 688.5 eV. Upon increasing the treatment time, a weak shoulder appears at low binding energies, indicating that different patterns can co-exist.[8,26]

Because valence electrons are involved in bond formation, subtle differences in surface chemistry may be obtained by studying the valence band region. The influence of the plasma treatment on the valence electronic states of the CNT is revealed by Figure 3, which summarizes the UPS valence band spectra obtained from five different samples: pristine MWCNTs and MWCNTs exposed to CF_4 plasma for 2, 30, 60 and 300 s.

The valence-band spectra were recorded using a photon with 110 eV of energy. The atomic subshell photoionization cross sections at this energy are 2 and 6×10^{-1} Mb for the 2p

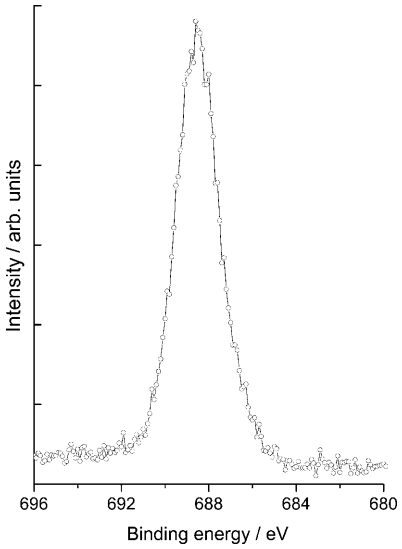

Figure 2. Fluorine 1s XPS spectrum recorded using $h\nu = 800$ eV on MWCNTs exposed to the CF_4 plasma functionalized for 300 s.

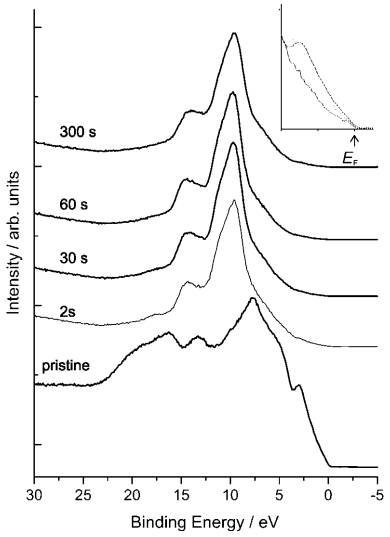

Figure 3. Valence band spectra recorded using $h\nu = 110$ eV on a) pristine MWCNTs compared with those CF_4-plasma treated for b) 2 s, c) 30 s, d) 60 s and d) 300 s. The inset shows the relative reduction of electronic states near the energy Fermi level.

and 2s fluorine states, and 2×10^{-1} and 4×10^{-1} for the 2p and 2s carbon states, respectively. The fluorine 2p cross section is higher than the carbon 2p cross section at this photon energy (~3 times higher),[19] so that the plasma-treated CNT spectrum is dominated by photoelectrons emitted from fluorine-derived electronic states.

The valence band structure of the pristine CNTs is characterized by features appearing close to 3.5 eV associated with photoelectrons emitted from the 2p–π band, extending from 5.5 to 8.0 eV associated with 2p–σ states and the mixed 2s–2p hybridized states at 13.6 eV. The σ–π hybridization resulting from the formation of the CNTs gives rise to the intensity at 11.5 eV.[27] The CNT spectrum is dominated by an intense C 2s region around 18 eV and a broad C 2p region in the range 9–15 eV.

The impact of the CF_4 plasma treatment on the CNT electronic valence states can be seen in the spectrum recorded on the sample treated for 2 seconds (Figure 3). Notably, the MWCNT electronic states are significantly attenuated. Photoelectrons emitted from the valence states of the plasma-treated samples generate new structures in the binding energy range of 5 to 16 eV. The broad feature appearing close to 8.3 eV was reported to be generated by photoelectrons emitted from anti-bonding orbitals of the C–F bonds with contribution of fluorine 2p states at high binding energy.[28] The main contribution of the photoelectrons emitted from the fluorine 2*p*-like states appears at 10 eV. The structure close to 15 eV originates from bonding orbitals of carbon 2s–F bonds.[28] The inset of Figure 3 shows that for increasing plasma treatment time, the relative intensity near 3.5 eV (associated with photoelectrons emitted from the 2p–π band of the CNTs) near the Fermi energy level is reduced. In agreement with results recently reported by Zhu, et al. showing that the field emission properties of CNTs can be enhanced or degraded depending on the CF_4 plasma parameters used,[29] the valence band modifications observed here suggest that fluorination can be used to tune electron emission characteristics by changing the density of electronic states near the Fermi energy level.

Having fully characterised the samples spectroscopically, we next turn to the possibility of surface defect identification using gold nanoclusters as markers. Figure 4a shows HRTEM

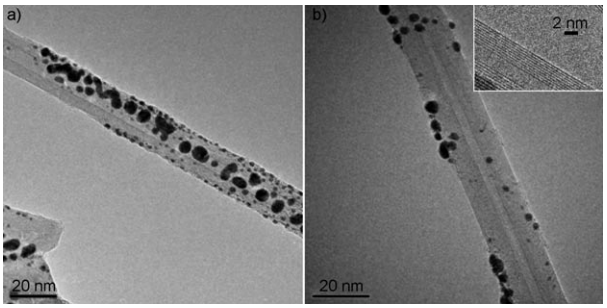

Figure 4. Gold clusters (black dots) at the CNT surface. a) Pristine CNT, b) nanotube exposed to CF_4 plasma for 30 s. Both samples received thermal evaporation of a nominal amount of 5 Å Au. As discussed in ref. [14], the nucleation of a metal cluster that weakly interacts with the CNT surface (such as gold) can be used to monitor the presence and dispersion of defects. The poor dispersion and small number of gold clusters in (b) suggests the absence of an excess of active sites for metal nucleation. The inset shows a magnified section of the CNT surface.

images of a pristine CNT after 5 Å of gold evaporation and Figure 4b the image recorded on plasma-functionalized CNTs (30 seconds followed by 5 Å of gold evaporation). In the inset, a high magnification illustrates the excellent state of the walls of the CNTs after the plasma treatment, indicating that, for the chosen parameters, the plasma treatment does not appear to damage the CNT surface.

As described by Fan, et al., the dispersion of a metal that weakly interacts with the CNT surface (such as gold) can be

used to monitor the presence of defects.[14] The gold evaporated onto pristine CNTs forms poorly dispersed clusters (Figure 4a) similar to those on the plasma-treated CNT (Figure 4b), suggesting that the plasma treatment performed using the current parameters does not create an excess of Au-trapping sites on the CNT surface.

In order to determine the exact nature of the gold-defect interaction, we performed a series of density functional calculations with a gold atom binding to various fluorine surface defects. Initially, we geometrically optimised two classes of fluorine defect on graphene, used as a simplified test system for a large-diameter nanotube. The first group consists of fluorine directly bound to a pristine surface—a single fluorine atom, a fluorine pair bonded to neighbouring carbon atoms [(1,2)-F_2 pair] and a fluorine pair bound to carbon atoms on opposite sides of the same hexagon in a third neighbour *cis* configuration [a (1,4)-F_2 pair], as shown in Figure 5a. The second group represent the surface-defect types that arise should the plasma start etching carbon from the nanotube surface, creating functionalised vacancies (vac), Figure 5b. The defects chosen were vac-F, similar in structure to the vacancy-oxygen structure (two carbon neighbours of the vacancy forming a weak reconstructed C–C bond, and the remaining under-coordinated carbon atom bonded directly to the fluorine atom), and vac-F_3, that is, a single fluorine atom added to each carbon neighbour of the vacancy. This second complex is highly strained due to the proximity of neighbouring fluorine atoms. There are other potential structures (such as vac_2-F_4) which could result from fluorine plasma etching, but we choose these two as representative.

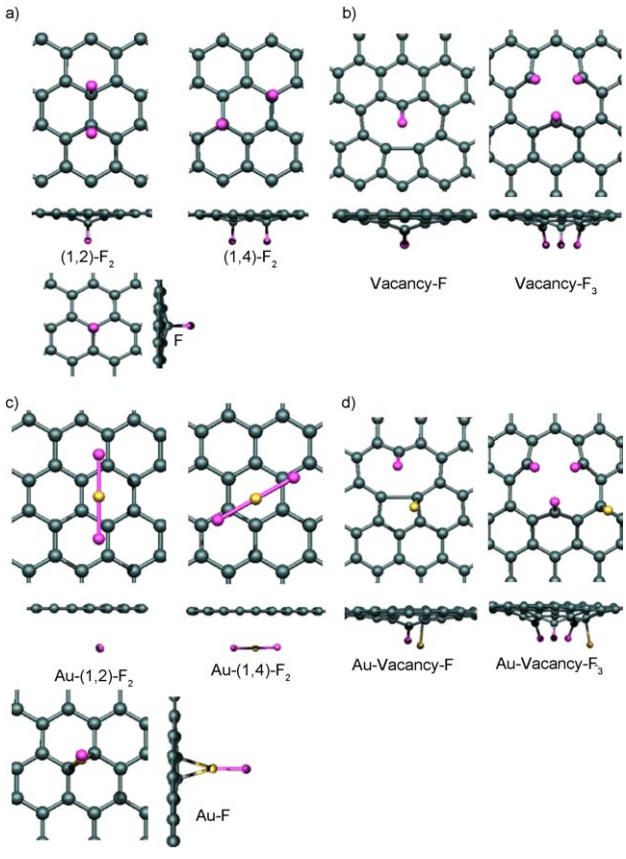

Figure 5. Fluorine and fluorine–gold complexes on graphene. a) F, (1,2)-F_2 and (1,4)-F_2 on pristine graphene, b) vacancy-F and vacancy-F_3 complexes, c) and d) The same species with a bound gold atom. Notably Au-F_2 debonds from the surface whereas in the presence of fluorinated vacancies gold remains weakly bound to the graphene surface. All structures are DFT geometrically optimised.

A single gold atom binds to a pristine graphene sheet with an energy of 0.65 eV, sitting directly above a carbon atom with Au–C bond length of 2.26 Å, and an excess electron spin of 0.99 μ_B. This atom is highly mobile, with a barrier of ~0.1 eV.[30] For the fluorinated vacancy structures, the calculations give behaviour very similar to that of gold interaction with oxygenated vacancies.[30] The gold sits above a carbon neighbour of the vacancy (Au–C bond length of 2.10 Å) with a binding energy of 1.35 eV for vac-F_3 and 1.29 eV for vac-F, that is, Au binding to the fluorinated vacancies is around 0.7 eV higher than to the pristine graphene surface (see Figure 5d). This implies that Au deposited on a surface containing fluorinated vacancies will rapidly migrate and be trapped at such sites, having to overcome a barrier of at least 0.8 eV to migrate away. The dwell time of Au atoms on such sites will therefore be much longer than on the basal plane and these sites will therefore act as nucleation centres for gold nanoparticle formation. Thus, on etched nanotube surfaces containing fluorinated vacancies, we might expect a very different gold particle distribution (smaller particles with more homogenous distribution) than on a pristine tube surface.

When the gold atom is geometrically optimised in a site next to fluorine bound to the basal plane we observe a very different response. In this case the gold forms strong Au–F bonds and the resultant complex (either Au–F or Au–F_2) lifts off the graphene surface with no energetic barrier (see Figure 5c). For both the (1,2)- and (1,4)-F_2 pair, the resultant Au–F_2 complex is completely debonded from the surface, lying parallel to the sheet over 3 Å above its surface (Au–F bonds of 1.95 Å). There is a strong energetic driving force for this process, with a net energy release of 2.92/2.99 eV [for (1,2)/(1,4)-F_2] compared to Au and F_2 bonded to the sheet in isolation. The Au–F complex remains slightly closer to the surface but is nonetheless still largely debonded, with a similar energetic driving force (2.2 eV), resulting in the Au sitting above a graphene bond with an F–C distance of 2.19 Å, and the fluorine atom a further 1.95 Å above that. In all of these cases we no longer have a covalently bound fluorine species on the basal plane, but instead a molecular Au–F_x complex sitting at the same distance or further from the graphene than the isolated Au atom. We would therefore expect a similar (high) mobility for such species.

Thus, we see an interesting phenomenon of graphene surface "cleaning" induced by the gold atom, whereby surface-bound fluorine atoms are debonded from the surface by the passage of the gold. In cases where fluorine is simply bound to the graphene basal plane with no carbon atom etching, we would therefore expect evaporated gold to behave closer to that for pristine tubes, with no preferential pinning sites and hence no change in gold nanoparticle size or distribution.

Since this is exactly the behaviour we see in the HRTEM images of nanotubes treated with low-plasma-power fluorine, we therefore conclude that we have not etched away carbon from the nanotube surface and are indeed bonding fluorine atoms directly to the basal plane. We note that majority peaks after rapid plasma treatment in the XPS spectra are associated with C_2F and C_4F coverage, consistent with the Au and theoretical results that the plasma is not etching the nanotube surface.

The use of graphene sheets in the calculations implies a lack of curvature; in small-radius single walled carbon nanotubes, surface fluorine binding is stronger and may not be so easily removed by gold.[31]

3. Conclusions

CF_4 rf plasma treatment of CNTs effectively grafts fluorine at the CNT surface, inducing changes in the CNT valence electronic states due to the formation of C–F bonds.

For increasing treatment time the relative intensity in the UPS spectra close to the Fermi energy level decreases suggesting that the functionalization of the CNT surface can be tailored. The fluorine atomic concentration depends on the plasma exposure time. The treatment does not significantly etch the CNT surface nor create active sites as evidenced the poor gold cluster dispersion.

DFT calculations confirm that gold on non-etched fluorinated surfaces is able to clean the surface by formation of metal–fluorine complexes which debond from the surface. Thus basal-plane bonded fluorine does not provide active pinning sites for gold. However fluorinated vacancies, which may be induced through the use of higher power fluorine plasmas, will act as active pinning sites for gold nanoparticle nucleation. Examination of gold nanoparticle size and distribution is therefore a powerful technique for direct analysis of the fluorination behaviour on the nanotube surface.

Acknowledgements

This work was supported by the Belgian Program on Interuniversity Attraction Pole (IUAP 6/08), ARC-UMH, and by the European Community—Research Infrastructure Action under the FP6 "Structuring the European Research Area" Programme (through the Integrated Infrastructure Initiative" Integrating Activity on Synchroton and Free Electron Laser Science—Contract R II 3-CT-2004-506008 (IASFS). The support of the BESSY staff and in particular of Dr. Willy Mahler, Dr. Birgitt Zada and Mr. Mike Sperling is gratefully acknowledged. G.V.L. acknowledges the Research Foundation—Flanders (FWO) for financial support as a Postdoctoral Research Fellow. C.P.E., I.S. and A.F. acknowledge EU Project "nano2hybrids" No. 033311 for funding. J.G. is a research associate of NFSR (Belgium).

Keywords: fluorine · gold · nanotubes · photoelectron spectroscopy · plasma chemistry

[1] A. Tressaud, E. Durand, C. Labrugère, *J. Fluorine Chem.* **2004**, *125*, 1639–1648.
[2] H. I. Bloemink, S. A. Cooke, J. H. Holloway, A. C. Legon, *Angew. Chem.* **1997**, *109*, 1399–1401; *Angew. Chem. Int. Ed. Engl.* **1997**, *36*, 1340–1342.
[3] K. H. An, J. G. Heo, K. G. Jeon, D. Bae, C. S. Jo, C. W. Yang, C. Y. Park, Y. H. Lee, Y. S. Lee, *Appl. Phys. Lett.* **2002**, *80*, 4235–4237.
[4] Y. S. Lee, T. H. Cho, B. K. Lee, J. S. Rho, K. H. An, Y. H. Lee, *J. Fluorine Chem.* **2003**, *120*, 99–104.
[5] E. T. Mickelson, C. B. Huffman, A. G. Rinzler, R. E. Smalley, R. H. Hauge, J. L. Margrave, *Chem. Phys. Lett.* **1998**, *296*, 188–194.
[6] H. Touhara, F. Okino, *Carbon* **2000**, *38*, 241–267.
[7] K. N. Kudin, H. F. Bettinger, G. E. Scuseria, *Phys. Rev. B* **2001**, *63*, 045413.
[8] C. P. Ewels, G. Van Lier, J. C. Charlier, M. I. Heggie, P. R. Briddon, *Phys. Rev. Lett.* **2006**, *96*, 216103.
[9] Z. Gu, H. Peng, R. H. Hauge, R. E. Smalley, J. L. Margrave, *Nano Lett.* **2002**, *2*, 1009–1013.
[10] A. Tressaud, E. Durand, C. Labrugère, *J. Fluorine Chem.* **2004**, *125*, 1639–1648.
[11] A. Felten, C. Bittencourt, J. J. Pireaux, G. Van Lier, J. C. Charlier, *J. Appl. Phys.* **2005**, *98*, 074308.
[12] S. Kaoru, S. Takeda, *Jpn. J. Appl. Phys. Part 1* **2007**, *46*, 7977–7982.
[13] A. Felten, J. Ghijsen, J. J. Pireaux, R. L. Johnson, C. M. Whelan, D. Liang, G. Van Tendeloo, C. Bittencourt, *Carbon* **2008**, *46*, 1271–1275.
[14] Y. Fan, B. R. Goldsmith, P. G. Collins, *Nat. Mater.* **2005**, *4*, 906–911.
[15] T. A. Witten, Jr., L. M. Sander, *Phys. Rev. Lett.* **1981**, *47*, 1400–1403.
[16] C. Kuhrt, M. Harsdorff, *Surf. Sci.* **1991**, *245*, 173–179.
[17] www.nanocyl.com.
[18] http://www.bessy.de/upload/bitpdfs/mustang.pdf.
[19] J. J. Yeh, I. Lindau, *At. Data Nucl. Data Tables* **1985**, *32*, 1–155.
[20] P. R. Briddon, R. Jones, *Phys. Status Solidi B* **2000**, *217*, 131–171.
[21] C. Hartwigsen, S. Goedecker, J. Hutter, *Phys. Rev. B* **1998**, *58*, 3641–3662.
[22] S. Hüfner, *Photoelectron Spectroscopy*, 3rd ed., Springer, Berlin, **2003**.
[23] Y. G. Wang, P. M. A. Sherwood, *Chem. Mater.* **2004**, *16*, 5427–5436.
[24] G. E. Nansé, P. Papirer, F. Fioux, A. Moguet, A. Tressaud, *Carbon* **1997**, *35*, 515–528.
[25] T. E. F. M. Standaert, M. Schaepkens, N. R. Rueger, P. G. M. Sebel, G. S. Oehrlein, J. M. J. Cook, *J. Vac. Sci. Technol. A* **1998**, *16*, 239–249.
[26] N. O. V. Plank, L. Jiang, R. Cheung, *Appl. Phys. Lett.* **2003**, *83*, 2426–2428.
[27] A. Felten, J. Ghijsen, J. J. Pireaux, R. L. Johnson, C. M. Whelan, D. Liang, G. Van Tendeloo, C. Bittencourt, *J. Phys. D* **2007**, *40*, 7379–7382.
[28] E. Morikawa, J. Choi, H. M. Manohara, H. Ishii, K. Seki, K. K. Okudaira, N. Ueno, *J. Appl. Phys.* **2000**, *87*, 4010–4016.
[29] Y. W. Zhu, F. C. Cheong, T. Yu, X. J. Xu, C. T. Lim, J. T. L. Thong, Z. X. Shen, C. K. Ong, Y. J. Liu, A. T. S. Wee, C. H. Sow, *Carbon* **2005**, *43*, 395–400.
[30] I. Suarez-Martinez, C. Bittencourt, X. Ke, A. Felten, J. J. Pireaux, J. Ghijsen, W. Drube, G. Van Tendeloo, C. P. Ewels, *Carbon*, DOI: 10.1016/j.carbon.2009.02.002.
[31] Y. Sato, M. Ootsubo, G. Yamamoto, G. Van Lier, M. Terrones, S. Hashiguchi, H. Kimura, A. Okubo, K. Motomiya, B. Jeyadevan, T. Hashida, K. Tohji, *ACS Nano* **2008**, *2*, 348–356.

Received: December 17, 2008
Revised: February 11, 2009
Published online on March 5, 2009

